Improved Crack Closure Line Position: An Improved Model for Crack Breathing Phenomenon

R. Ramezanpour, M. Ghayour and S. Ziaei-Rad

Department of Mechanical Engineering, Isfahan University of Technology 84156-83111 Isfahan, Iran

(Received 3 October 2012; accepted 15 November 2013)

The dynamic behaviour of a cracked Jeffcott rotor is investigated in this paper. The crack is located at the midpoint of the rotor. It is known that when the static deflection dominates the vibration of the rotating shaft, the crack opens and closes according to the shaft rotation. This phenomenon is known as crack breathing. There are several models for classifying crack breathing phenomena, such as the switching crack model, harmonic approach model, and response-dependent breathing crack model. In order to model the breathing of the crack in the response-dependent breathing crack model, the concept of a crack closure line position (CCLP) is proposed and used by some researchers. The main scope of this work is to present an improved crack closure line position (ICCLP). By using several contour plots over the crack's surface, it is shown that the imaginary line that separates the open and closed parts of a breathing crack should not be considered perpendicular to the crack tip. It is also shown that the improved model positively agrees with those proposed in the literature. The effects of ICCLP on the coefficients of the local flexibility matrix are investigated.

NOMENCLATURE

Symb.	Unit	Description
I	m^4	area moment of inertia for the cross section
k_{ij}	N/m, N/rad	cross-coupled stiffness
dp	m	disk diameter
e	m	eccentricity
$[k]_g$		global stiffness matrix
φ	rad	initial phase angle
$[c]_l$		local flexibility matrix of the cracked shaft
m	kg	mass of the disk
ν		Poisson ratio
R, d	m	radius and diameter of the shaft, respectively
α	rad	rotor center displacement in rotational direction
l	m	shaft length
k_x	N/m	stiffness in x direction
k_y	N/m	stiffness in y direction
k_u	N/m	stiffness in longitudinal direction
k_T	N/rad	stiffness in torsional direction
W	Nm	strain energy due to crack
U	Nm	strain energy of uncracked shaft
t	s	time in seconds
$[C_s]$		total flexibility matrix of the uncracked shaft
$[K]_l$		local stiffness matrix
η_0	m	location of elemental strip along η' direction
$[H]$		transformation matrix
h	m	height of the element strip
J_p	m^2	polar moment of inertia for the cross section
q_1	N	longitudinal force (internal reaction)
c	Ns/m	transversal damping coefficient
E	N/m^2	modulus of elasticity
q_4, q_5	Nm	bending moments (internal reactions)
c_T	Ns/rad	torsional damping coefficient
γ	m	crack depth
Ω	rpm	revolutionary speed
c_u	Ns/m	longitudinal damping coefficient
$M(t)$	Nm	external torsional excitation
G	N/m^2	modulus of rigidity
ω_T	rpm	torsional excitation frequency
A	m^2	cross sectional area of the crack
x, y	m	transversal displacements of center of disk
u	m	longitudinal displacement of center of disk
α	rad	torsional displacement of center of disk
F_z	N	longitudinal force (external load)
T	Nm	torsional moment
J	kgm^2	mass moment of inertia of the disk
K_{I}^i	$N/m\sqrt{m}$	opening mode of the crack due to internal load "i"
K_{III}^j	$N/m\sqrt{m}$	tearing mode of the crack due to internal load "j"
K_{I}	$N/m\sqrt{m}$	total opening mode of the crack
K_{III}	$N/m\sqrt{m}$	total tearing mode of the crack
F_1, F_2, F_{III}		influential functions

1. INTRODUCTION

Many investigations have been conducted concerning the overall behaviour of cracked shafts in past decades. In general, a crack in rotating shafts may be classified in three different ways: opened crack, closed crack, and breathing crack. In other words, if a cracked shaft rotates under external loading, then the crack opens and closes regularly per revolution, which could be said to breathe. This phenomenon is produced

by the stress distribution around the crack.[1] This is a very common situation in large turbine-generator rotors.[2] Throughout the two past decades, the main focus of some studies was the modelling and explanation of the breathing mechanism in cracked shafts.[3–14] Georgantzinos et al. investigated the time history of local flexibilities associated with a breathing crack in a rotating shaft.[1] The deflections of a beam with a circular cross-section presenting a crack of different depths was analysed using quasi-static approximation with the aid of a refined nonlinear contact-finite element. The partial contact of crack surfaces was predicted by using this method. In his excellent review paper, Papadopoulos explained many crack models, such as the open crack model, switching crack model, second moment inertia model, breathing models, and harmonic model approaches.[2] The use of strain energy release rate theory (SERR) and its combination with linear fracture mechanics and rotor dynamics for calculating the compliance matrix have been considered in detail.

Dimarogonas and Papadopoulos conducted an analysis of a cracked rotor neglecting the non-linear behaviour of the crack by assuming a constant stiffness asymmetry and using the theory of shafts with dissimilar moments of inertia.[6] Later, they derived a complete flexibility matrix of the cross-section containing the crack.[7] Grabowski suggested switching the stiffness values, from those of an uncracked rotor (closed crack state) with those of a cracked rotor (fully open state) at a particular angular position of the rotor (when the crack edge becomes vertical).[8] Mayes and Davies suggested sinusoidal stiffness variations to model the breathing in a more sensible way, as a rotor crack is expected to open and close gradually due to gravity.[9] Papadopoulos and Dimarogonas represented stiffness variation by means of a truncated, four term series using known stiffness matrices corresponding to half-open, half-closed, fully open, and fully closed cracks.[10] Changhe et al. represented the crack as a hinge with variable stiffness in two rotor-fixed lateral directions.[11] The crack is introduced at the node of a finite element model. Ballo investigated the flexural vibrations of a continuous slender shaft with a crack.[12] The mathematical model of the problem has been formulated by means of the finite element method. However, the crack was modelled by a switching crack. It has been shown that the increase in crack depth causes a decrease in the bending stiffness, whereas the nonlinearity is related to the opening and closing of the crack faces in the process of flexural vibrations. Subsequently, the theoretical results have been illustrated by the calculation of the amplitudes and phases of the second and third harmonics of the forced shaft flexural vibrations. Darpe et al. proposed a response-dependent non-linear breathing crack model, which is called crack closure line position (CCLP).[13] Considering all six degrees of freedom per node, the stiffness matrix in a Timoshenko beam element is modified to account for the effect of the crack. Using this model, they were able to study the coupling between longitudinal, lateral, and torsional vibrations. They observed that motion coupling, together with the rotational effect of the rotor and non-linearities due to their proposed breathing model, introduced sum and difference frequency in the response of the cracked rotor. Bachschmid et al. used a 3D FE model to investigate the breathing mechanism in a rotating shaft.[14] Slant and helicoidally cracks are the two types of crack shape models that they considered. A simplified model to determine the open area of a crack is also presented in their work. This simple model has been used for analysing the non-linear dynamic behaviour of cracked rotating shafts, which occurs when breathing is governed by the vibration itself. It has been concluded that torsional deflections could be generated by bending moments due to the coupling effects.

Additionally, the response of a cracked rotor is investigated in some of the literature. Sekhar investigated the dynamic behaviour of a cracked rotor—in particular, that of a rotor with two open transverse cracks.[15] The influence of one crack over the other was studied using finite element analysis while considering flexural vibrations. Darpe et al. investigated a simple Jeffcott rotor with two transverse surface cracks.[16] However, they assumed that one crack remains open while the other is breathing. Also, the effect of the interaction of two cracks on the breathing behaviour and on the unbalanced response of the rotor was studied. They observed significant changes in the dynamic response of the rotor when the angular orientation of one crack relative to the other is varied. Darpe et al. presented a novel way to detect fatigue transverse cracks in rotating shafts.[17] In this technique, a transient torsional excitation was applied for a very short duration at a specific angular orientation of the rotor, and then the transient features of the resonant bending vibration were revealed using wavelet transform. Subsequently the sensitivity of the proposed methodology to the depth of crack is investigated. It is mentioned that this detection method is very specific to the behaviour of the transverse surface crack in a horizontal rotor. Fortunately, a positive feature of their proposed method was that the response features were different from the responses of other common rotor faults under similar excitation. Lin and Chu investigated the dynamic behaviour of a slant (45^o crack angle) cracked rotor.[18] Using the Jeffcott rotor model, the equation of motion was extracted in four directions. The global stiffness of the system was obtained from concepts of fracture mechanics and strain energy release rate. They mentioned that a much longer time is required to compute the steady responses of a breathing cracked shaft than that of an open cracked shaft and that this is why almost all investigators have adopted the open crack model. The existence of the frequency of torsional excitation is included in the longitudinal response, and the combined frequencies of the rotating frequency and the frequency of torsional excitation in the transverse response are good indicators for slant crack detection.

By using several contour plots over the crack surface, it is shown in this paper that the imaginary line (crack closure line) that separates the open and closed parts of a breathing crack should not be considered perpendicular to the crack tip. According to these plots, a new breathing model called the improved crack closure line position (ICCLP) is introduced. Using the proposed model, the dynamic behaviour of a cracked Jeffcott rotor is considered. The effect of this model on the flexibility of the cracked shaft is investigated in detail. Subsequently, steady state responses and their spectrums are investigated.

2. EQUATIONS OF MOTION

Consider a Jeffcott rotor rotating at speed Ω (Fig. 1). It has a massless shaft and a disk with mass m. A view of the cross-section of the disk is shown in Fig. 2. In this figure, XOY is the stationary coordinate, $\xi o \eta$ is the rotational coordinate with

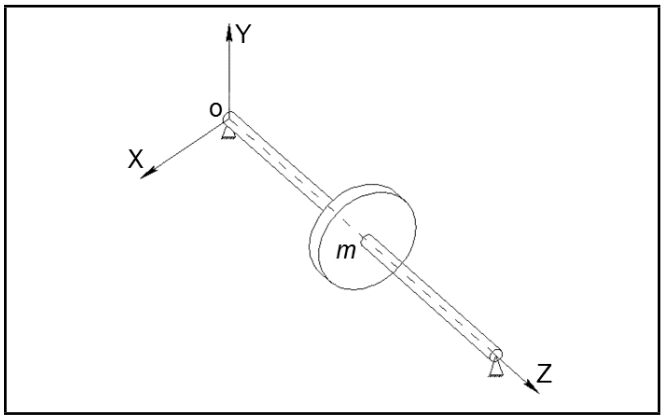

Figure 1. Jeffcott rotor model.

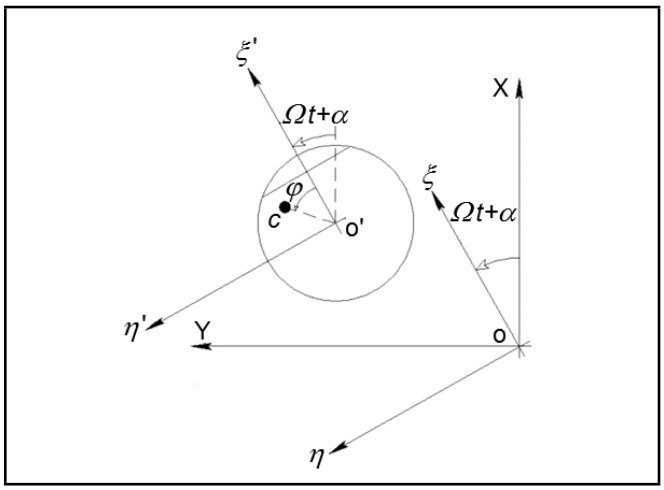

Figure 2. Cross-sectional view of crack at midpoint of the shaft.

centre o, and $\xi' o' \eta'$ is the rotational coordinate that is attached at the centre of the disk. Coordinate o' is the centre of the disk, c is the centre of mass of the disk, α is the angle that is caused by torsional vibration, and φ is the phase angle of the centre of mass.

The angle position of the centre of mass is

$$\Theta = \Omega t + \alpha + \varphi; \tag{1}$$

then

$$\dot{\Theta} = \Omega + \dot{\alpha}, \qquad \ddot{\Theta} = \ddot{\alpha}. \tag{2}$$

Using the d'Alambert principle (Fig. 3), the equation of motion in four directions (two transverse, one torsional, and one longitudinal) can be established as

$$m\ddot{x} + c\dot{x} + k_x x + k_{xy} y + k_{xT}\alpha + k_{xu} u = -mg + me\,(\Omega+\dot{\alpha})^2 \cos(\Omega t+\alpha+\varphi) + me\ddot{\alpha}\sin(\Omega t+\alpha+\varphi); \tag{3}$$

$$m\ddot{y} + c\dot{y} + k_{xy} x + k_y y + k_{yT}\alpha + k_{yu} u = me\,(\Omega+\dot{\alpha})^2 \sin(\Omega t+\alpha+\varphi) - me\ddot{\alpha}\cos(\Omega t+\alpha+\varphi); \tag{4}$$

$$J\ddot{\alpha} + c_T(\Omega+\dot{\alpha}) + k_{xT} x + k_{yT} y + k_T\alpha + k_{Tu} u = M(t) + mge\sin(\Omega t+\alpha+\varphi) + me\ddot{x}\sin(\Omega t+\alpha+\varphi) - me\ddot{y}\cos(\Omega t+\alpha+\varphi); \tag{5}$$

$$m\ddot{u} + c_u\dot{u} + k_{xu} x + k_{yu} y + k_{Tu}\alpha + k_u u = 0; \tag{6}$$

where J is the mass moment of inertia of the disk, about o'. The damping coefficients in the transverse, torsional, and longitudinal directions are shown by c, c_T, and c_u, respectively. It

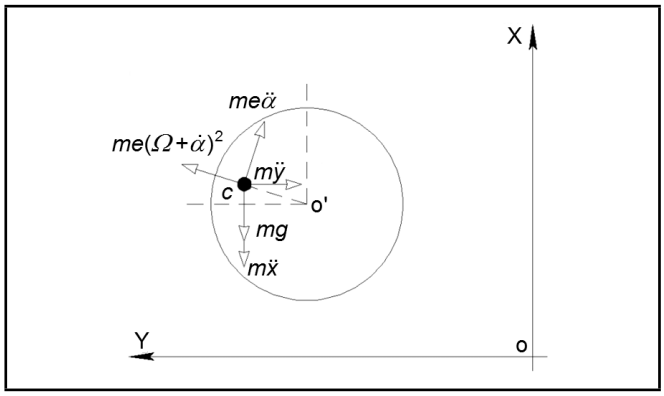

Figure 3. Forces on the centre of mass of the disk.

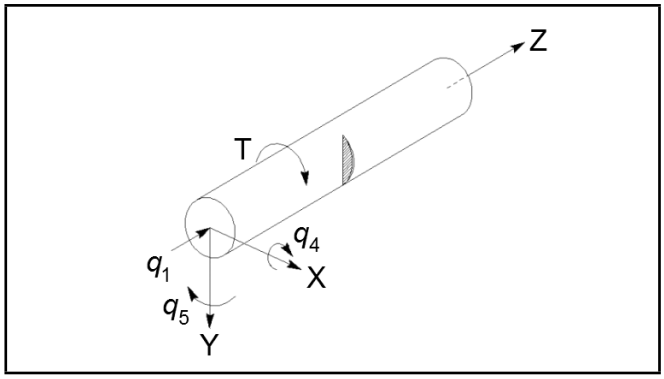

Figure 4. Internal reactions on the crack.

should be mentioned that these equations are the same as those presented in the work of Lin and Chu.[18] $M(t)$ and e denote the torsional excitation and eccentricity of the disk, respectively. Using Eqs. (3)–(6), the stiffness matrix of the system can be determined as

$$[k]_g = \begin{bmatrix} k_x & k_{xy} & k_{xT} & k_{xu} \\ k_{xy} & k_y & k_{yT} & k_{yu} \\ k_{xT} & k_{yT} & k_T & k_{Tu} \\ k_{xu} & k_{yu} & k_{Tu} & k_u \end{bmatrix}. \tag{7}$$

3. FLEXIBILITY OF A CRACKED ROTOR

Suppose that the internal reactions on the crack are two bending moments q_4 and q_5, one torsional moment T, and one longitudinal force q_1 (Fig. 4). Using Castiglione's theorem, the local flexibility of the crack can be written as

$$[c]_l = [G_1][\Delta c_{ij}][G_2] + [C_s]; \tag{8}$$

where

$$\Delta c_{ij} = \frac{\partial^2 W}{\partial q_i \partial q_j}, \quad [G_1] = \left[\frac{l}{4}, \frac{l}{4}, 1, 1\right], \quad [G_2] = \left[\frac{l}{4}, \frac{l}{4}, 1, 1\right], \quad [C_s] = \mathrm{diag}\left(\frac{l^3}{48EI}, \frac{l^3}{48EI}, \frac{l}{2GJ_p}, \frac{l}{2AE}\right). \tag{9}$$

In Eq. (9), W is the additional strain energy due to the crack. It is obvious that local flexibility of the crack is determined if additional stain energy due to the crack is known, and it can be expressed as

$$W = \int_A J(A)\, dA; \tag{10}$$

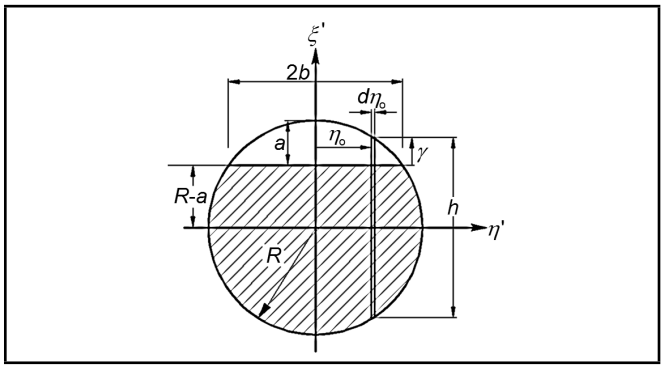

Figure 5. Crack surface.

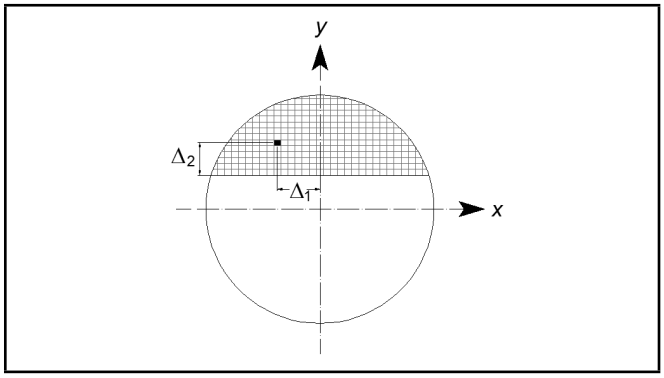

Figure 6. Mesh over the crack surface for evaluation of first mode over the cracked surface.

where $J(A)$ is the strain energy density function. In general, $J(A)$ is a function of K_{I}, K_{II}, and K_{III}, which are the stress intensity factors for the opening mode, sliding mode, and tearing mode, respectively. But here, K_{II} (sliding mode) is neglected. Thus,

$$J = \frac{1}{E'}\left[K_{\mathrm{I}}^2 + (1+\nu)K_{\mathrm{III}}^2\right]; \tag{11}$$

where $E' = \frac{E}{1-\nu^2}$ and ν is the Poisson's ratio. Therefore, according to Eqs. (10) and (11), the additional strain energy due to the crack can be written as

$$W = \int_A \frac{1}{E'}\left[K_{\mathrm{I}}^2 + (1+\nu)K_{\mathrm{III}}^2\right] dA; \tag{12}$$

where A is total surface of the crack for the third crack mode (K_{III}), and the opening part of the surface of crack for the first crack mode (K_{I}).[18]

The crack surface is shown in Fig. 5. Therefore, the stress intensity factors (SIF) for a transverse crack are
for q_1,

$$K_{\mathrm{I}}^1 = \frac{q_1}{\pi R^2}\sqrt{\pi\gamma}F_1; \tag{13}$$

$$K_{\mathrm{III}}^1 = 0; \tag{14}$$

for q_4,

$$K_{\mathrm{I}}^4 = \frac{4q_4\eta_0}{\pi R^4}\sqrt{\pi\gamma}F_1; \tag{15}$$

$$K_{\mathrm{III}}^4 = 0; \tag{16}$$

for q_5,

$$K_{\mathrm{I}}^5 = \frac{4q_5\sqrt{R^2-\eta_0^2}}{\pi R^4}\sqrt{\pi\gamma}F_2; \tag{17}$$

$$K_{\mathrm{III}}^4 = 0; \tag{18}$$

and for T,

$$K_{\mathrm{I}}^T = 0; \tag{19}$$

$$K_{\mathrm{III}}^T = \frac{2T\sqrt{R^2-\eta_0^2}}{\pi R^4}\sqrt{\pi\gamma}F_{\mathrm{III}}. \tag{20}$$

It should be noted that the total effect of q_4 is zero.[18] According to Tada et al.,[19]

$$F_1 = \sqrt{\frac{\tan(\lambda)}{\lambda}}\left[0.752 + 1.01\frac{\gamma}{\sqrt{R^2-\eta_0^2}} + 0.37\left(1-\sin(\lambda)\right)^3\right]\frac{1}{\cos(\lambda)}; \tag{21a}$$

$$F_2 = \sqrt{\frac{\tan(\lambda)}{\lambda}}\left[0.923 + 0.199\left(1-\sin(\lambda)\right)^4\right]\frac{1}{\cos(\lambda)}; \tag{21b}$$

$$F_{\mathrm{III}} = \sqrt{\frac{\tan(\lambda)}{\lambda}}; \tag{21c}$$

where

$$\lambda = \frac{\pi\gamma}{4\sqrt{R^2-\eta_0^2}}. \tag{21d}$$

Therefore, the total strain density functions are

$$K_{\mathrm{I}} = \left(\frac{q_1}{\pi R^2}F_1 + \frac{4q_4\eta_0}{\pi R^4}F_1 + \frac{4q_5\sqrt{R^2-\eta_0^2}}{\pi R^4}F_2\right)\sqrt{\pi\gamma}; \tag{22}$$

$$K_{\mathrm{III}} = \left(\frac{2T\sqrt{R^2-x_0^2}}{\pi R^4}\right)\sqrt{\pi\gamma}F_{\mathrm{III}}. \tag{23}$$

After calculating the local flexibility of the cracked rotor, the local stiffness of the system can easily be calculated as

$$[K]_l = [c]_l^{-1}; \tag{24}$$

and the global stiffness matrix in the inertia coordinate system is

$$[K]_g = [H]^{-1}[K]_l[H]; \tag{25}$$

where

$$[H] = \begin{bmatrix} \cos(\Phi) & \sin(\Phi) & 0 & 0 \\ -\sin(\Phi) & \cos(\Phi) & 0 & 0 \\ 0 & 0 & 1 & 0 \\ 0 & 0 & 0 & 1 \end{bmatrix}, \quad \Phi = \Omega t + \alpha. \tag{26}$$

4. CONSTANT K_{I} CONTOURS OVER THE CRACK SURFACE

In order to use the CCLP model, the value of stress intensity factor in the first mode (K_{I}) is evaluated over the crack tip.[13] The change in the sign of K_{I} shows the position of CCLP, which is assumed to be perpendicular to the crack tip. Therefore, CCLP separates the crack area into two parts: open and closed. In this paper, it is shown that the line that separates the crack surfaces is not perpendicular to the crack tip. A meshed example that has been used here for drawing constant K_{I} contours is shown in Fig. 6. According to Eq. (22), it is obvious that the value of K_{I} is dependent on the values of q_1, q_4, and q_5. Therefore, in order to draw the contours, one is required

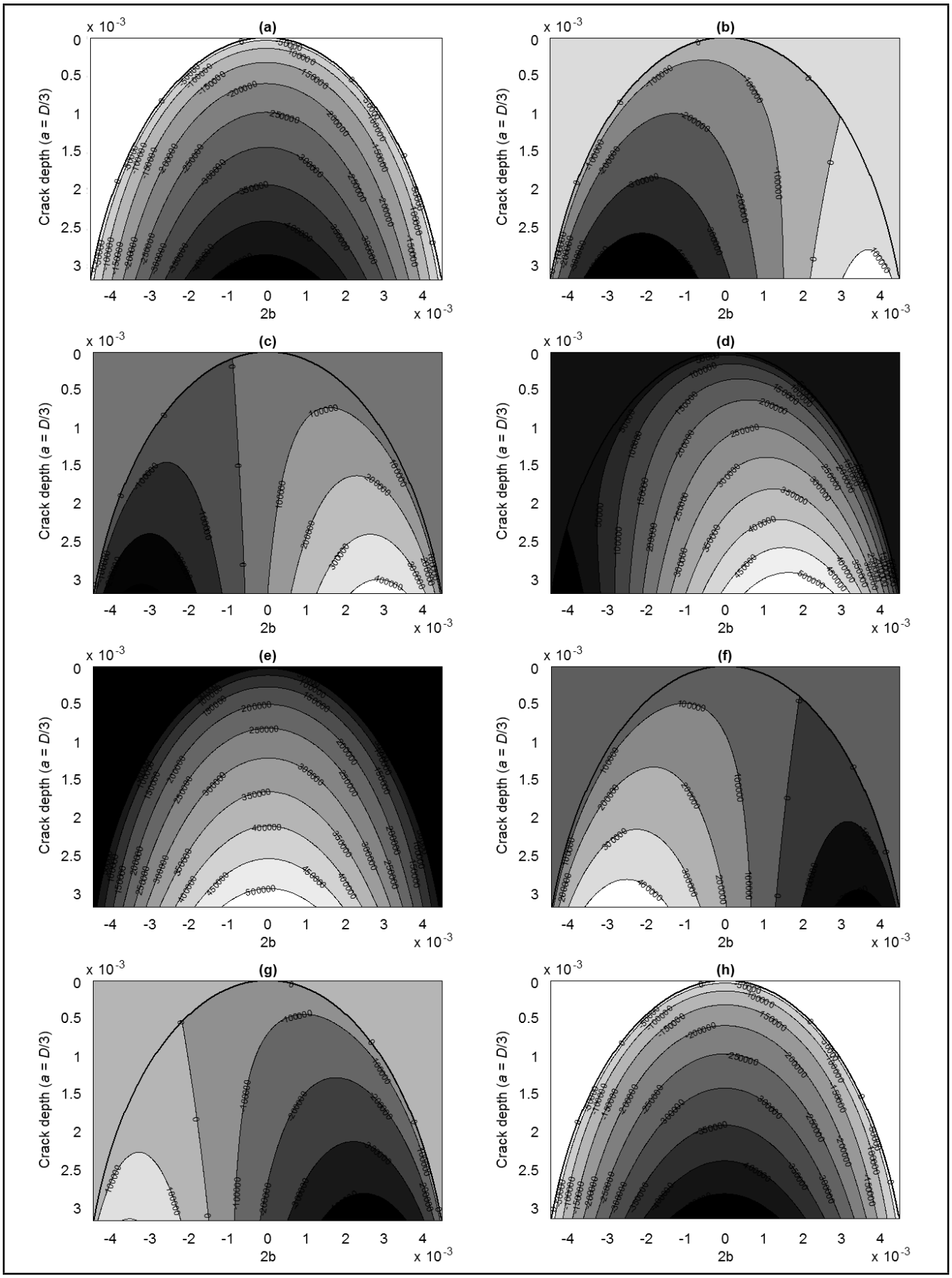

Figure 7. Contours over the crack surface for (a) 0º, (b) 50º, (c) 100º, (d) 150º, (e) 180º, (f) 250º, (g) 300º, and (h) 360º.

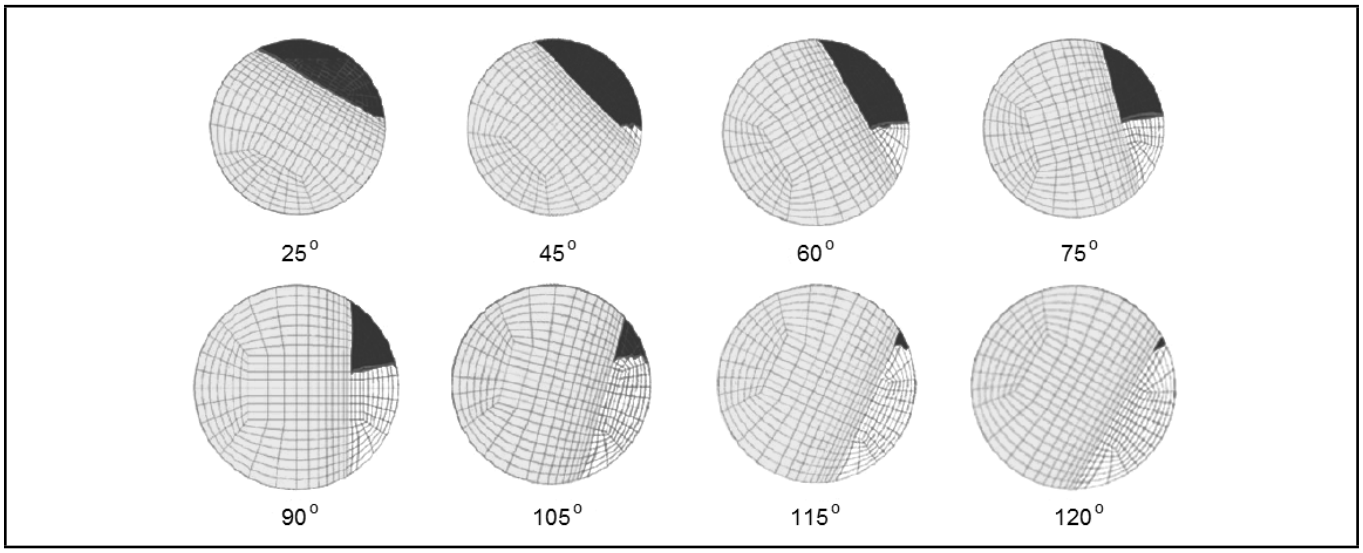

Figure 8. Open and closed areas in different angular positions.[14]

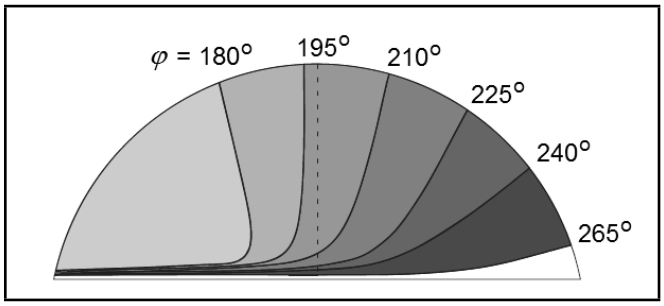

Figure 9. Evolution of contact area between the crack surfaces for a transverse crack under bending.[1]

to solve the equation of motion. On the other hand, the determination of the solution needs the computation of q_1, q_4, and q_5. In fact, drawing the constant K_{I} is an interdependent procedure. This procedure is explained here. Using the Runge-Kutta numerical method, the equations of motion are solved for Δt time intervals, which is related to the time that is needed for one degree rotation of the rotor. Therefore, the values of forces on the crack surface are known. So K_{I} is a function of η and γ which are the distances from the vertical axis (Δ_1) and crack depth line (Δ_2), respectively (see Fig. 6).

Suppose that in the initial situation the crack is closed due to the weight of the rotor; so in $t = 0$, the stiffness of the system is known, and thus the solving of the equations of motion is possible. It should be noted that, in general, the stiffness of a cracked rotor system with a closed crack is not equal to the stiffness of an uncracked rotor. Figure 7 shows the constant K_{I} contours over the crack surface for 0°, 50°, 100°, 150°, 180°, 250°, 300°, and 360°. Figure 2(b) shows the length of the crack depth line. According to this figure, two crack surfaces coincide with each other at the zero rotation angle. In other words, the crack is closed, and therefore all contours have negative values, which show that the two crack surfaces are in compression. Due to an increase in the value of the rotation angle, the crack opens gradually. Therefore, the values on some contours are positive while the others are negative. As one can see, the contour with zero value separates the open and closed parts on the crack surface. At the 90° rotation angle (which is not presented here in Fig. 7), the open and closed parts of the crack separate from each other with a straight line that is perpendicular to the crack tip. In a similar way, due to the increase in the value of the rotation angle, the contour with zero value travels to the left side of the crack surface. So at the 180° rotation angle, all the contours have positive values (which means that the crack is fully open). By increasing the value of the rotation angle further than 180°, contours with zero value travel from the right side to the left side of the crack surface. Here, the contours that are situated on the right side of the zero contour have a negative sign, and the contours that are situated in the left side of the zero contour have a positive sign. This means that the right side of the crack is closing while the left side of it is opening. At the 360° rotation angle, the whole crack surface is closed, similar to the zero angle. Figure 7 shows that the separation boundary is not always a straight line, while this boundary in the CCLP model has been considered as a straight line.[13] Also, it is obvious that this boundary is not perpendicular to the crack tip as has been assumed for the CCLP model. Bachschmid et al. investigated the breathing phenomenon in detail using 3D nonlinear FEM.[14] The open and closed parts of the crack surface during the rotation of the rotor are presented in their work (Fig. 8). According to this figure, the boundary between the open and closed parts of the crack surface is not a straight line. Furthermore, this boundary is not perpendicular to the crack tip. One can therefore claim that these two results are in good agreement to those presented in this section. Figure 9 shows the results that are presented by Georgantzinos and Anifantis, which is evaluated due to bending moments only.[1]

It is obvious that the results presented in Fig. 9 are not the same as those are obtained in this paper. However, the overall schematic of the results are in good agreement with each other.

5. ICCLP MODEL

As mentioned in the previous section, the contour with zero value is the separation curve that separates the open and closed surfaces of the breathing crack from each other. Therefore, the introduced model can be called crack closure curve position (CCCP) (Fig. 10).

According to Fig. 10, the integration in Eq. (12) should be calculated over the ACBD area. Since the determination of the ACBD curve—from every degree of rotation—is almost im-

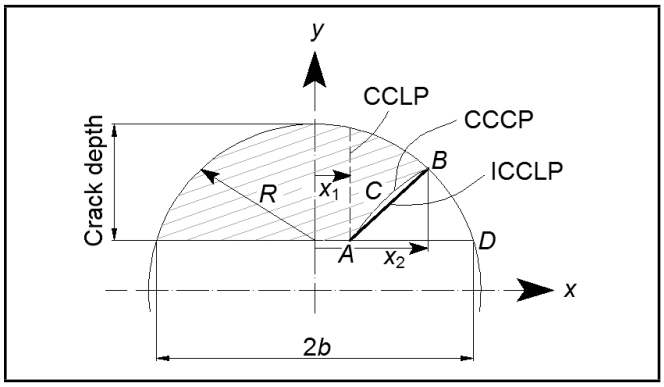

Figure 10. Difference in the location of CCCP, CCLP, and ICCLP.

possible, the curve ACB is approximated by the AB line. This means that the integration in Eq. (12) should be calculated over the ABD area. Due to this approximation, a new breathing model is introduced and is called the ICCLP. Figure 10 shows the position of CCCP and ICCLP. Figure 11 shows the variations of the elements of the $[\Delta c_{ij}]$ matrix for a crack depth $a = D/3$ and $D = 9.5$ mm.

In Fig. 11, the dashed lines express the ICCLP model, and the continuous lines express the CCLP model. It should be noted that the horizontal axis shows the variations of the position of point A, or the CCLP (Fig. 10). According to Fig. 11, the values of compliance, which are calculated with the ICCLP model, are different from those calculated with the CCLP model.

As it is shown in Fig. 12, for CCLPs less than 90°, the amount of the open area of the crack that is bounded by the ICCLP model is less than that bound by the CCLP model. Therefore, compliances that are calculated with the CCLP model are greater than those calculated with the ICCLP model. Also, according to Fig. 12, it is obvious that for CCLPs between 90° and 180°, the values of compliance for the ICCLP model are greater than the values of compliance calculated with the CCLP model. For CCLPs between 180° and 270°, the values of compliance that are calculated with the ICCLP model are greater than those calculated with the CCLP model. However, for CCLPs between 270° and 360°, it is the reverse. It should be noted that Fig. 11 shows that the use of the ICCLP or CCLP models does not change the value of some of the compliance elements, such as $c(1,3)$, $c(2,3)$, and $c(3,4)$. According to Eq. (22), it is obvious that T does not contribute in K_{I}, so the value of $c(3,3)$ is not sensitive to the position of point A; therefore, the value of $c(3,3)$ for CCLP and ICCLP models is the same. Similarly, the values of $c(1,3)$, $c(2,3)$, and $c(3,4)$ are equal to zero for both CCLP and ICCLP models. However, it should be mentioned that K_{III} is not zero for $c(3,3)$, while for $c(1,3)$, $c(2,3)$, and $c(3,4)$ it is zero.

6. NUMERICAL SIMULATION

The parameters that are needed for solving the equations of motion are summarised in Table 1.

A program has been written in the MATLAB® environment to estimate the response of a transverse cracked rotor using the ICCLP model for crack breathing. The solution process for using the model mentioned is presented in Fig. 13. According to this flowchart, the initial displacement is assumed to be equal to the static deflection of the uncracked rotor and the initial

Table 1. Characteristics of the studied rotor system.

Speed of revolution	$\Omega = 500$ rpm
Torsional excitation freq.	$\omega_T = 0.6\Omega = 300$ rpm
External torsional excitation	$M_T = \sin(\omega_T t)$
Transverse damp coefficient	$c = 41.65$ kg/s
Torsional damp coefficient	$c_T = 0.0091$ kgm^2/s
Longitudinal damp coefficient	$c_u = 146.2034$ kg/s
Modulus of elasticity	$E = 210$ GPa
Disk mass	$m = 0.595$ kg
Shaft length	$l = 0.26$ m
Shaft diameter	$d = 9.5$ mm
Disk diameter	$dp = 76$ mm
Initial phase angle	$\varphi = \pi/6$ rad
Poisson's ratio	$\nu = 0.3$
Eccentricity	$e = 0.1643$ mm

stiffness values correspond to that of the cracked rotor. Rotational speed (Ω) and $t_{\max}$, corresponding to total time of solution, are known. Knowing the shaft rotational speed, the time for one degree rotation can be calculated. Using the procedure mentioned (Fig. 13), the program evaluates the forces that act on the crack surfaces. Thus, by using these forces, stress intensity factors (SIFs) are evaluated at points along the crack. Changes in the sign of the SIF over the crack tip determines the position of point A.

Elements of the stiffness matrix for the CCLP model can be evaluated using this point. Also, the position of point B is identified using the zero contour of K_{I} over the crack surface, and therefore, the stiffness of the system that is calculated for the CCLP model is corrected for the ICCLP model. The equation of motion is solved for the Δt time interval by using this stiffness matrix, which is assumed to be constant for one degree of rotation. For the next step, this time increment will increase by Δt, and then the forces that act on the crack will be evaluated. The equations of motion will be calculated for the present step using these forces. This iterative procedure will be repeated until the total time ("t") is greater than or equal to $t_{\max}$. There are two points that should be mentioned about the proposed algorithm: the $t_{\max}$ parameter should be adopted in such a way that guarantees the steady state response of the system; the second point concerns the selection of the time step in the Runge-Kutta numerical method, which should be set in small increments. The small time steps guarantee insignificant changes in the response of the system. In Fig. 13, the steps that are embedded in the program for the ICCLP method are determined by dashed lines. In fact, if this part is removed from the flowchart, the remaining algorithm can be used for the CCLP method. As previously mentioned, in order to determine the position of point B, the contours of K_{I} should be calculated for the crack surface. It is obvious that the calculation of these contours is a time consuming procedure, particularly due to the fact that it should be carried out for every rotation angle. This is why the time required for the ICCLP model is greater than that is for the CCLP model.

Figure 14 shows the non-dimensional position of points A and B (Fig. 10) versus the rotor rotation angle under steady state conditions. According to Fig. 14, for rotation angles of less than 90° (and also between 180° and 270°), the position of point B is always on the right side of point A, which indicates that the separation line is not perpendicular to the crack tip. However, for rotation angles between 90° and 180° (and between 270° and 360°), the position of point B is always on the left side of the position of point A. For angles equal to 0°,

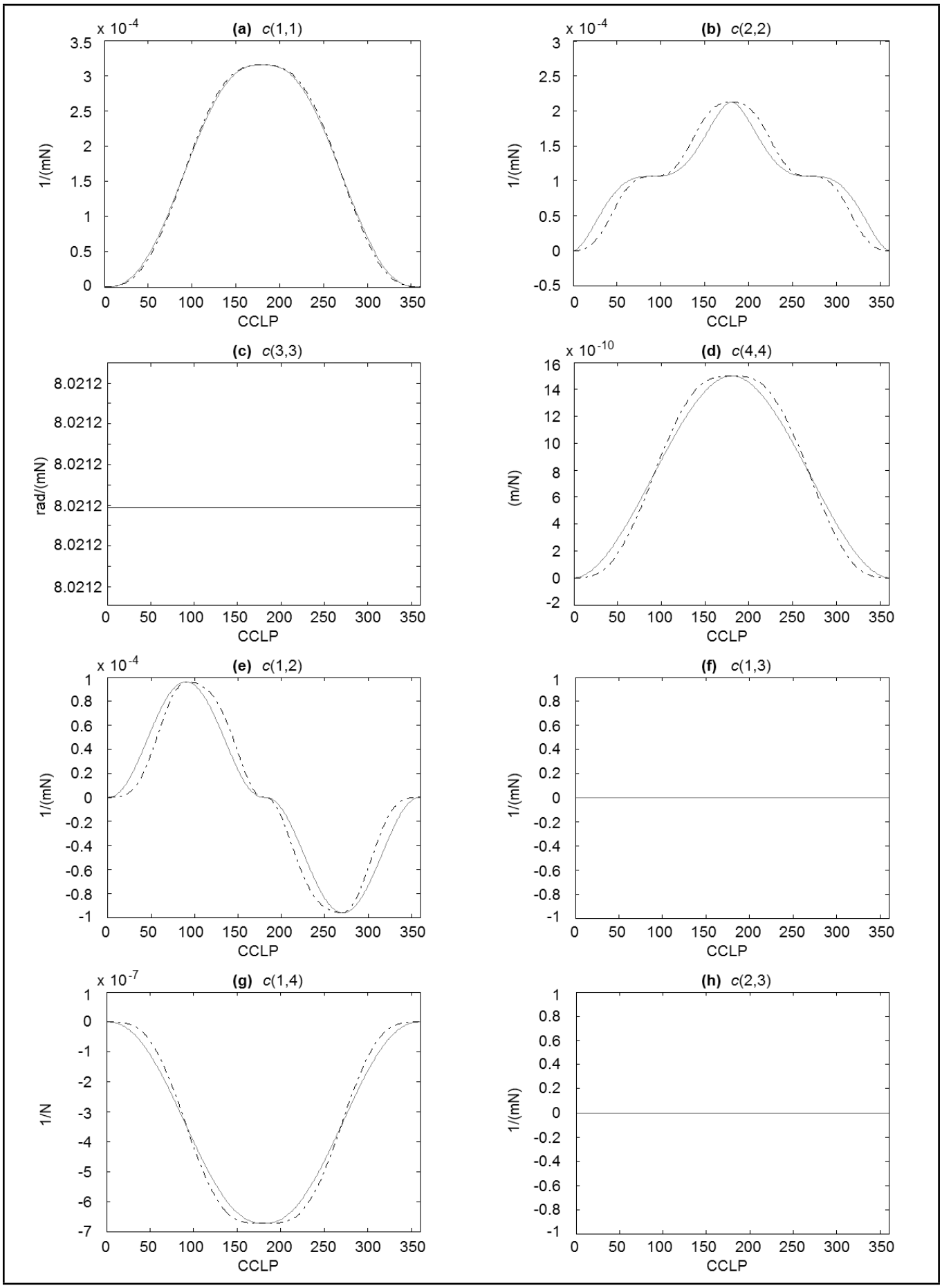

Figure 11. Variations of the elements of the $[\Delta c_{ij}]$ matrix for a crack depth $a = D/3$ and $D = 9.5$ mm; continuous line: CCLP model; dashed line: ICCLP. (a) $c(1,1)$, (b) $c(2,2)$, (c) $c(3,3)$, (d) $c(4,4)$, (e) $c(1,2)$, (f) $c(1,3)$, (g) $c(1,4)$, (h) $c(2,3)$, (i) $c(2,4)$, and (j) $c(3,4)$.

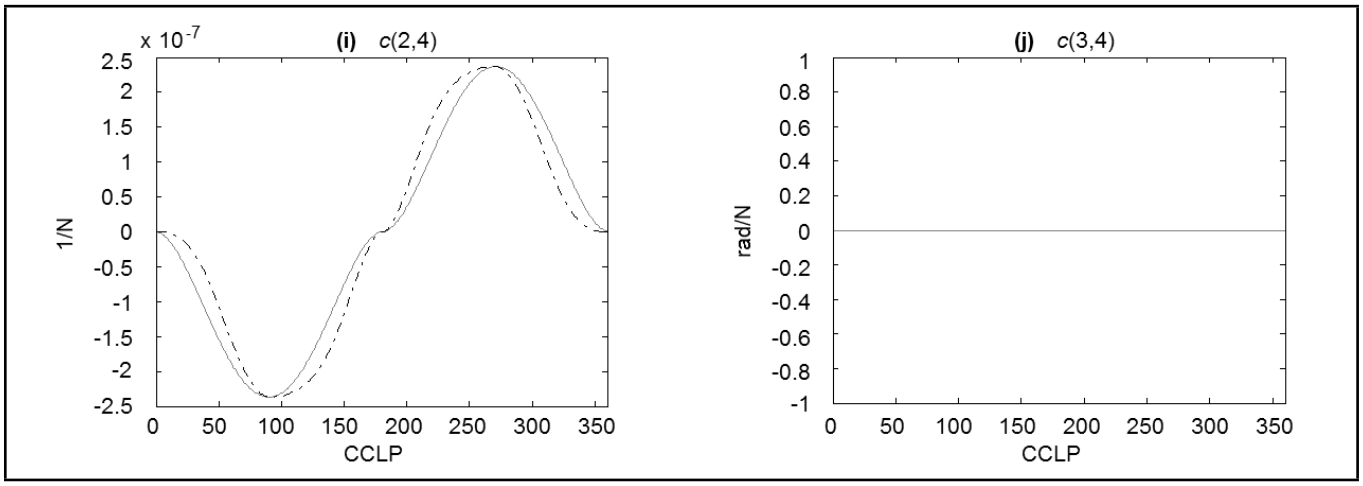

Figure 11. (cont.) Variations of the elements of the $[\Delta c_{ij}]$ matrix for a crack depth $a = D/3$ and $D = 9.5$ mm; continuous line: CCLP model; dashed line: ICCLP. (a) $c(1,1)$, (b) $c(2,2)$, (c) $c(3,3)$, (d) $c(4,4)$, (e) $c(1,2)$, (f) $c(1,3)$, (g) $c(1,4)$, (h) $c(2,3)$, (i) $c(2,4)$, and (j) $c(3,4)$.

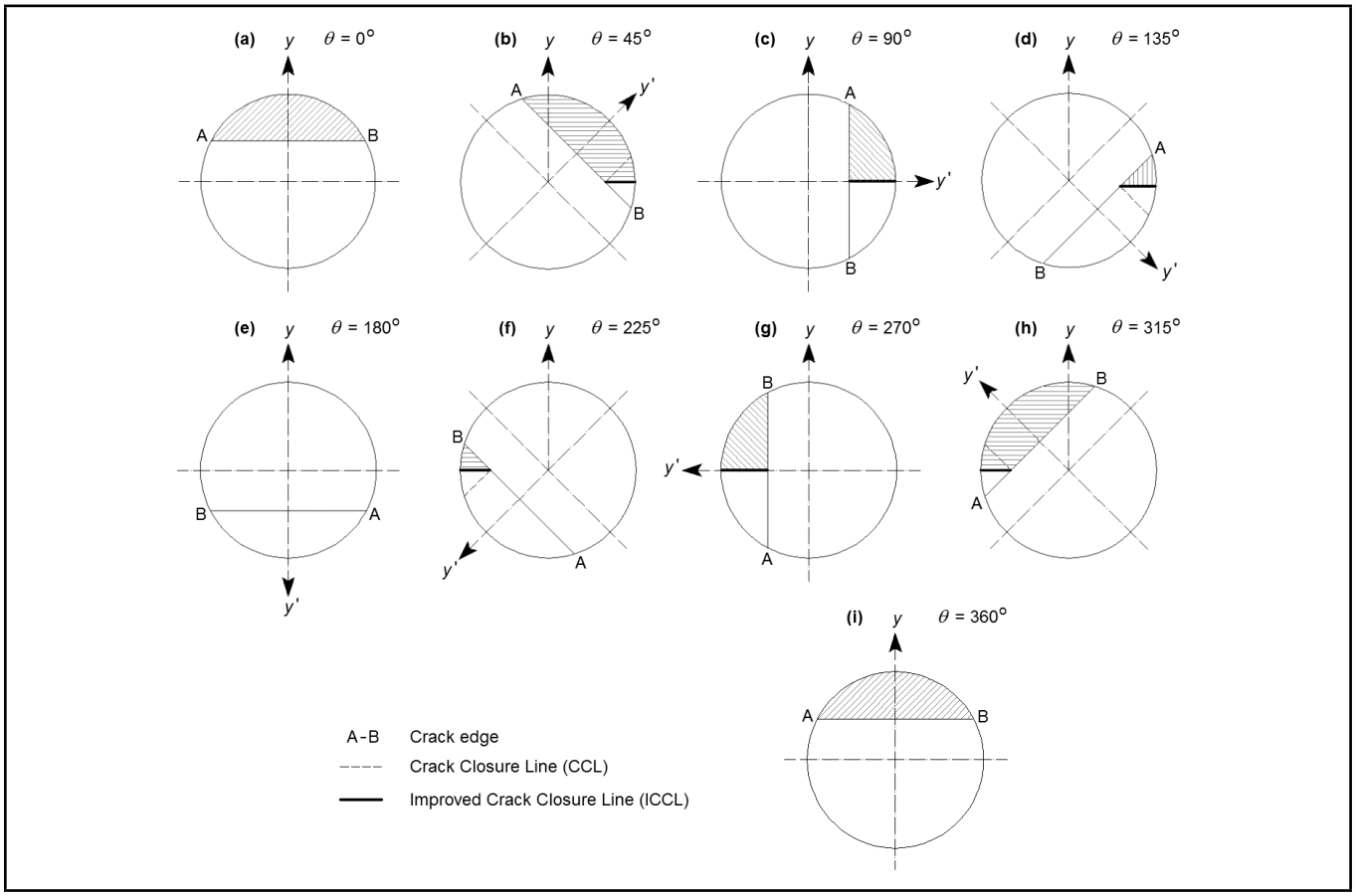

Figure 12. Comparison between ICCLP and CCLP from Darpe et al.[13]

90°, 180°, 270°, and 360°, points A and B coincide with each other. This is why the values of the crack compliance matrix for these angles are the same for the models of CCLP and ICCLP. However, for angles of 90° and 180°, the open and closed parts of the crack area are equal to each other.

Figure 15 shows the time domain steady state responses for the cracked shaft with a transverse crack for four directions (i.e. two transverse, one torsional, and one longitudinal). In Fig. 15, the horizontal axis is the time (in seconds) and the vertical axis is the magnitude of the responses (in metres for transverse and longitudinal responses and in radians for the torsional response). These responses are evaluated for a cracked Jeffcott rotor ($\alpha = a/D$). Furthermore, a continuous line identifies the CCLP model and a dashed line identifies the ICCLP model.

According to Fig. 15, in general, the time responses for the two models are not the same. In other words, except for the torsional response, the other responses in transverse and longitudinal directions are different. The response in the torsional direction is the same for two models, and this can be explained

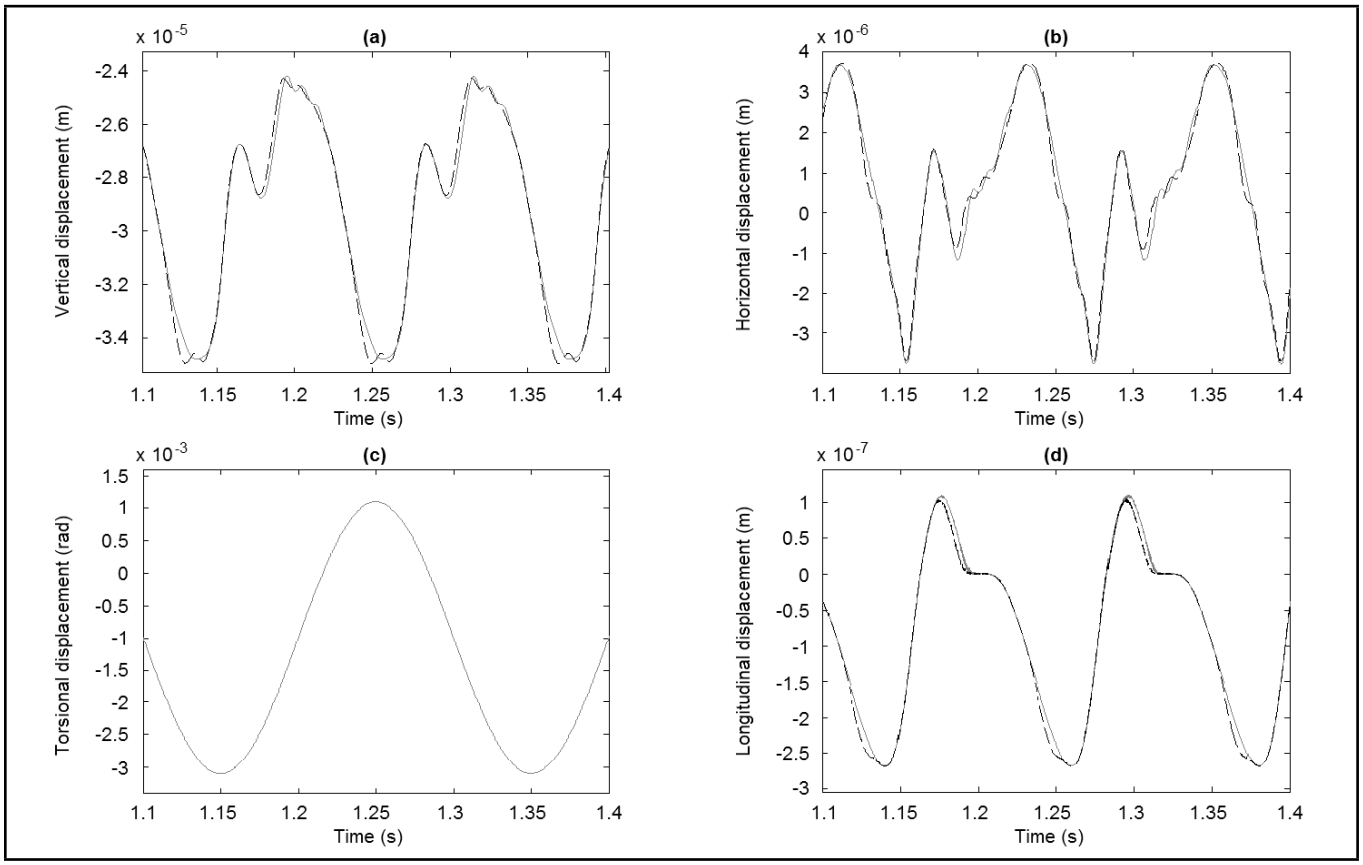

Figure 15. Time domain steady state responses for the cracked shaft with a transverse crack. Continuous line: CCLP model; dashed line: ICCLP model. (a) Vertical displacement, (b) Horizontal displacement, (c) Torsional displacement, and (d) Longitudinal displacement.

by using Fig. 11. According to this figure, the elements that are related to torsional direction—i.e. $c(1,3)$, $c(2,3)$, $c(3,3)$, and $c(3,4)$—are zero and are thus the same for the two models. Therefore, the two models show the same behaviour, as can be seen in Fig. 15(c). Figure 16 displays a comparison between the amplitude-frequency spectrums of the steady state responses of the shaft with respect to the two crack breathing models (i.e. CCLP and ICCLP). In this figure, the horizontal axis is the frequency (revolutions per minute), and the vertical axis is the log scale of amplitude (metres or radians). According to this figure, the frequency components of the responses are the same for the CCLP and ICCLP models. Furthermore, there is no difference between the torsional spectrums for CCLP and ICCLP models. In fact, they are coincident with each other. However there is a slight difference in the amplitude of the spectrums of the responses (except for the torsional response). It can be seen that by increasing the frequency, the difference between the amplitudes of the responses calculated by the two models also increases. Figure 17 identifies the reason for this. According to this figure, the difference between the amplitudes of the frequency components is observable, especially at high frequencies. In summary, the use of the two models for crack breathing discussed has no effect on the frequency components of the responses, but changes in the amplitude of the spectrums is apparent in some high frequencies.

7. CONCLUSIONS

In this paper, the dynamic behaviour of a cracked Jeffcott rotor has been investigated. The main scope of this work is to modify the existing breathing model. Using several contour plots over the crack surface, it has been shown that CCLP, which separates the open and closed parts of a breathing crack, cannot be considered perpendicular to the crack tip. A new breathing model—ICCLP—was introduced and showed that the results obtained are in good agreement with those proposed in the literature. The effects of ICCLP on the coefficients of the local flexibility matrix have also been investigated.

It is concluded that the value of the element of the crack compliance matrix is not equal for CCLP and ICCLP; it depends on the value of the crack rotation angle when the rotor in under steady state conditions.

The time response and frequency response of the system have been compared. It is shown that there are differences between the responses obtained from the two models. It was observed that when the value of the frequency increases, the difference between the amplitudes of the responses computed from the two models also increases.

REFERENCES

[1] Georgantzinos, S. K. and Anifantis, N. K. An insight into the breathing mechanism of a crack in a rotating shaft, *Journal of Sound and Vibration*, **318** (1–2), 279–295, (2008).

[2] Papadopoulos, C. A. The strain energy release approach for modeling cracks in rotors: A state of the art review, *Mechanical Systems and Signal Processing*, **22** (4), 763–789, (2008).

[3] Papadopoulos, C. A. and Dimarogonas, A. D. Stability of cracked rotors in the coupled vibration mode, *Journal*

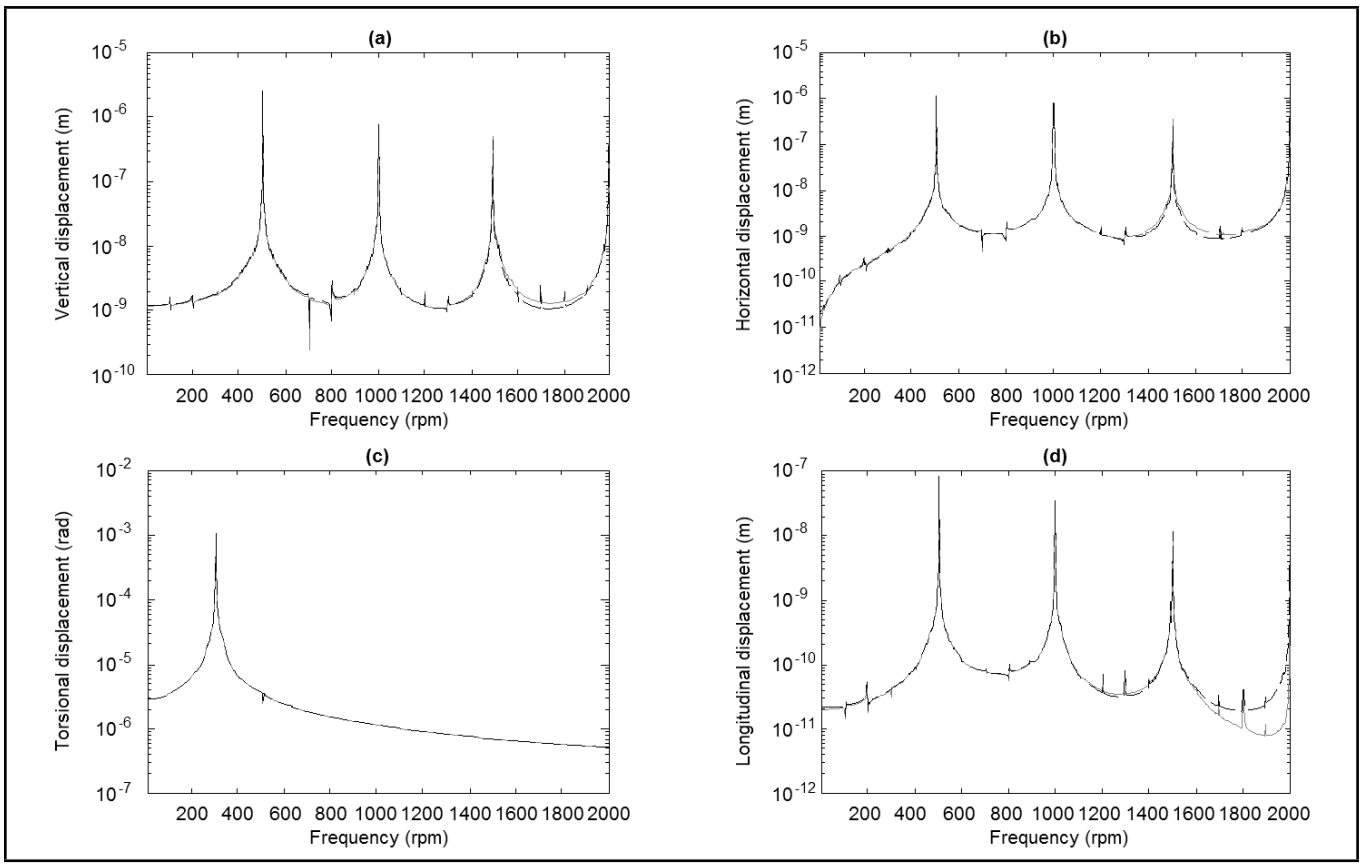

Figure 16. Comparison between amplitude-frequency spectrums of steady state responses of the shaft with respect to two crack breathing models: CCLP and ICCLP. (a) Vertical displacement, (b) Horizontal displacement, (c) Torsional displacement, and (d) Longitudinal displacement. Continuous line: CCLP model; dashed line: ICCLP.

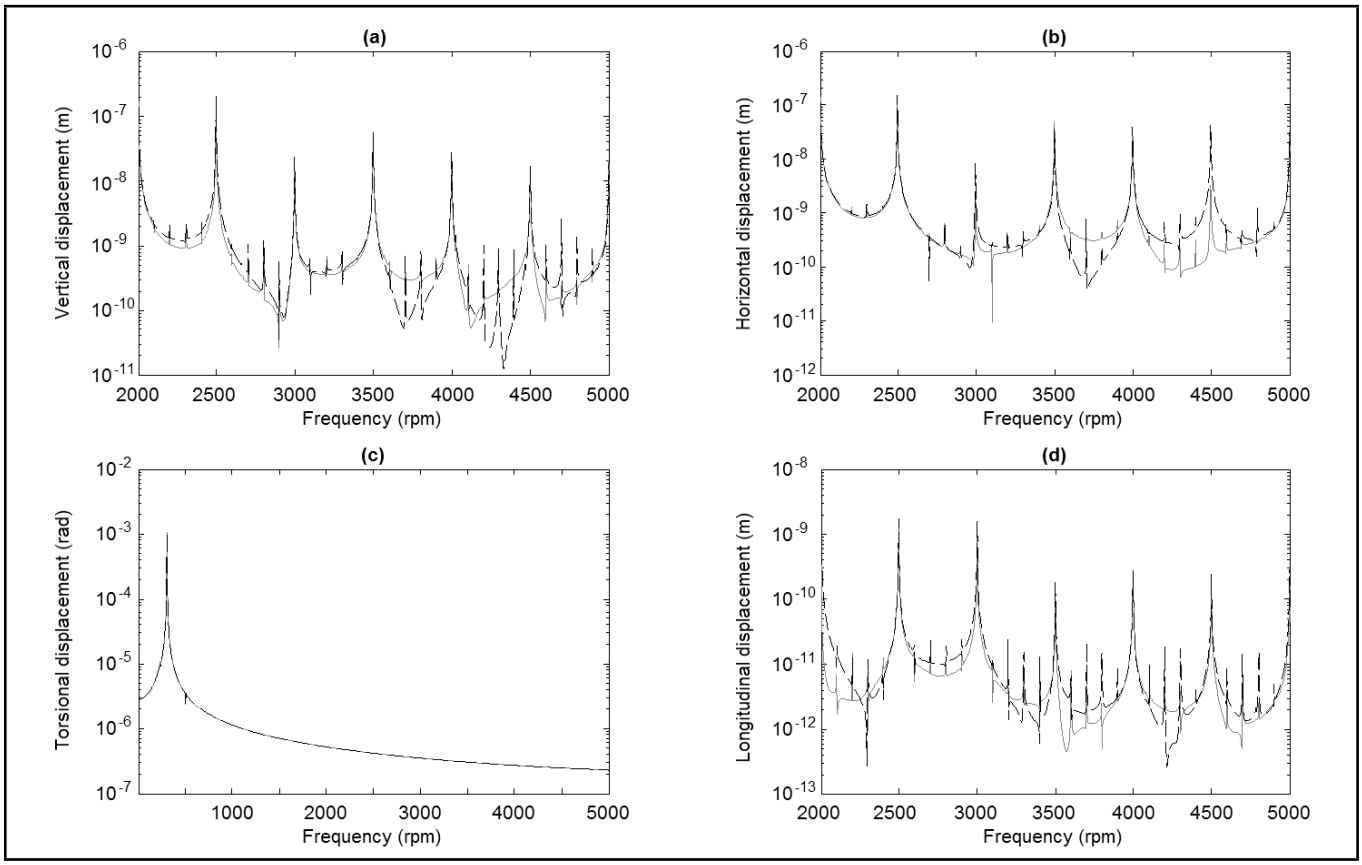

Figure 17. Comparison between amplitude-frequency spectrums of steady state responses of the shaft with respect to two crack breathing models: CCLP and ICCLP. (a) Vertical displacement, (b) Horizontal displacement, (c) Torsional displacement, and (d) Longitudinal displacement. Continuous line: CCLP model; dashed line: ICCLP.

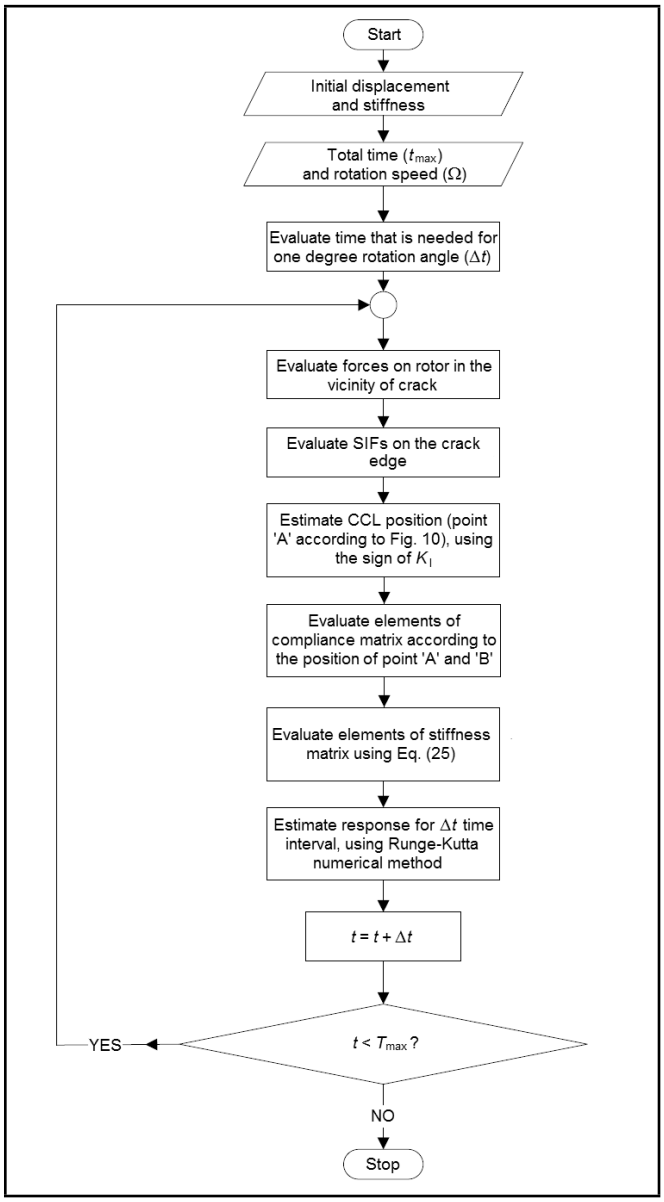

Figure 13. Solution procedure used in the numerical process.

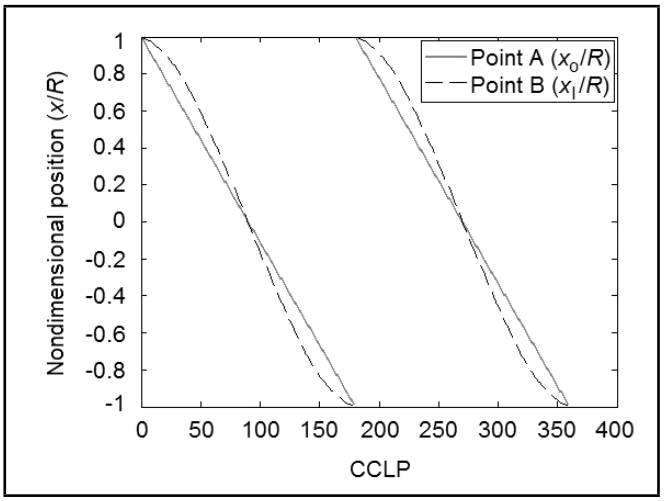

Figure 14. Non-dimensional position of point A and B versus rotor rotation angle. Continuous line: point A; dashed line: point B.

of Vibration, Acoustics, Stress, and Reliability in Design, **110** (3), 356–359, (1988).

[4] Wauer, J. Modeling and formulation of equations of motion for cracked rotating shafts, *International Journal of Solids and Structures*, **26** (8), 901–914, (1990).

[5] Jun, O. S., Eun, H. J., and Earmme, Y. Y. Modeling and vibration analysis of a simple rotor with a breathing crack, *Journal of Sound and Vibration*, **155** (2), 273–290, (1992).

[6] Dimarogonas, A. D. and Papadopoulos, C. A. Vibration of cracked shafts in bending, *Journal of Sound and Vibration*, **91** (4), 583–593, (1983).

[7] Papadopoulos, C. A. and Dimarogonas, A. D. Coupled longitudinal and bending vibrations of a rotating shaft with an open crack, *Journal of Sound and Vibration*, **117** (1), 81–93, (1987).

[8] Grabowski, B. *The vibrational behaviour of a rotating shaft containing a transverse crack*, O. Mahrenholtz (Ed.), Springer Press, (1984).

[9] Mayes, I. W. and Davies, W. G. R. Analysis of the response of a multi-rotor-bearing system containing a transverse crack in a rotor, *Journal of Vibration, Acoustics, Stress, and Reliability in Design*, **106**, 139–145, (1984).

[10] Papadopoulos, C. A. and Dimaragonas, A. D. Stability of cracked rotors in the coupled vibration mode, *Journal of Vibration, Acoustics, Stress, and Reliability in Design*, **110**, 356–359, (1988).

[11] Changhe, L., Bernasconi, O., and Xenophontidis, N. A generalized approach to the dynamics of cracked shafts, *Journal of Vibration, Acoustics, Stress, and Reliability in Design*, **111** (3), 257–263, (1989).

[12] Ballo, I. Non-linear effects of vibration of a continuous transverse cracked slender shaft, *Journal of Sound and Vibration*, **217** (2), 321–333, (1998).

[13] Darpe, A. K., Gupta, K., and Chawla, A. Coupled bending, longitudinal and torsional vibrations of a cracked rotor, *Journal of Sound and Vibration*, **269** (1–2), 33–60, (2004).

[14] Bachschmid, N., Pennacchi, P., and Tanzi, E. Some remarks on breathing mechanism, on non-linear effects and on slant and helicoidal cracks, *Mechanical Systems and Signal Processing*, **22** (4), 879–904, (2008).

[15] Sekhar, A. S. Vibration characteristics of a cracked rotor with two open cracks, *Journal of Sound and Vibration*, **223** (4), 497–512, (1999).

[16] Darpe, A. K., Gupta, K., and Chawla, A. Dynamics of a two cracked rotor, *Journal of Sound and Vibration*, **259** (3), 649–675, (2003).

[17] Darpe, A. K. A novel way to detect transverse surface crack in a rotating shaft, *Journal of Sound and Vibration*, **305** (1–2), 151–171, (2004).

[18] Lin, Y. and Chu, F. The dynamic behavior of a rotor system with a slant crack on the shaft, *Mechanical Systems and Signal Processing*, **24** (2), 522–545, (2010).

[19] Tada, H., Paris, H., and Irwin, G. R. *The stress analysis of cracks*, Professional Engineering Publishing, (2000).